ISSN 1330-3651 (Print), ISSN 1848-6339 (Online) https://doi.org/10.17559/TV-20211011140249
Preliminary communication

High Embankment Dam Stability Analysis Using Artificial Neural Networks

Milica MARKOVIC*, Novak RADIVOJEVIC, Miona ANDREJEVIC STOSOVIC, Jelena MARKOVIC BRANKOVIC, Srdjan ZIVKOVIC

Abstract: Regular surveillance, data acquisition, and visual observation of high embankment dams are extremely important for the stability analysis of these structures. The stability issues that could occur during a dam's lifetime are mainly related to slope instability and internal erosion. The aim of continuous dam security monitoring and field measurement is to identify priority flow paths in the dam body, i.e. cracks and the erosion process. A key parameter for embankment dam stability assessment is the pore water pressure (PWP) response in the clay core. Increasing pore water pressure results in shear strength reduction and can cause dam instability. In this paper, four different models based on artificial neural networks will be developed for pore water pressure prediction in an embankment dam clay core, based on meteorological, hydrological, and geotechnical data. These models will be compared and the model that gives the smallest prediction error will be presented. In the light of climate change, the main objective of this paper is to find the model that can be used for embankment dam stability prediction in extreme weather events.

Keywords: artificial neural network; embankment dam; pore water pressure; stability analysis

1 INTRODUCTION

Embankment rockfill dams are the most common dam construction types used in the world today [1].

Surveillance and visual observation of high dams is extremely important for safety analysis, since most of these structures are old and have been in an operating period for several decades [2].

The embankment dam stability issues that could occur during a dam's lifetime are mainly related to slope instability and internal erosion [3].

Based on statistical data, embankment dam failure causes (52,5%) are mainly permeability damage and piping [4].

Pore water pressure, otherwise known as formation pressure, corresponds to hydraulic potential and refers to the pressure of groundwater within the soil, in the pores [5]. In embankment dams it depends on the water level in the reservoir.

In light of climate change, when flood waves are becoming more frequent and unpredictable, old dam stability can be significantly compromised.

The pore water pressure response is fundamental for dam stability since its increase results in shear strength reduction, and can cause dam instability [6].

Additionally, from the aspect of dynamic load, liquefaction can inflict a lot of problems on embankment dams.

During earthquakes over the last decades (e.g. Christchurch 2011, Emilia 2012, Palu 2018), liquefaction, or softening of the soil due to pore pressure build up, and decrease of shear strength caused serious damage to the structures.

Excess pore pressure prediction is fundamental for embankment dam seismic safety as well [7].

The aim of continuous embankment dam monitoring and field measurement is to identify priority flow paths in the dam body, which means cracks and the erosion process.

The main indicator of these potential processes is seepage flow on the downstream face of a dam, springs, and a wet area with significant greenery.

On the other hand, the amount of silt soil particles in the seepage water is a significant indicator of reduction of water tightness as well [3].

Field measurement of pore pressure in an embankment dam can reliably provide information about ongoing seepage processes in the dam, soil mechanical properties of the dam body, and hydraulic conditions [8].

Embankment dam stability analysis, regarding the pore-pressure problem, has been addressed by many authors [9]-11].

Pore pressure prediction (i.e. dam safety prediction) can be conducted using different methods, by finding a correlation between various parameters and pore pressure [5].

Different prediction models of pore water pressure have been developed based on physical laws, with analytical [12][13] and numerical solutions [14][15].

Artificial Intelligence (AI) is a scientific approach in engineering and refers to the simulation of human intelligence in machines. Under AI one can find many available tools such as artificial neural networks, a radial basis function, fuzzy logic, support vector machines, and functional networks [5].

Ahmed in paper [5] developed a model for pore pressure prediction based on drilling parameters and log data (weight on bit, rotary speed and rate of penetration, mud weight, bulk density, porosity, and compressional time).

In our paper, four different structures of artificial neural networks were explored to obtain the best model for pore pressure prediction for the rockfill dam Bovan.

The objective of this paper is to apply and compare these models.

This prediction is based on available hydrological, meteorological and geotechnical data, such as the water level in the reservoir, the piezometer water level, and air temperature.

Pore pressure measured over a certain number of previous days is also considered. The measured dataset for the period from November 5th to October 1st in 2019 and 2020 was used.

A common multi-layer perceptron (MLP) was used, as well as a standard recurrent neural network (RNN), long short-term memory (LSTM), and a gated recurrent unit (GRU) with a different number of inputs. The outcome of this study can provide suggestions for the system that best predicts dam safety.

2 METHODOLOGY

2.1 The Multilayer Perceptron (MLP)

All the neurons within an MLP are grouped into layers. There is one input layer, one output layer, and an arbitrary number of hidden layers located between the input and output layer.

An arbitrary number of neurons can be found in each layer, where each neuron in one layer is connected by weight connections to each neuron in the next layer.

The activation of one neuron is obtained by applying the activation function (sigmoid function, ReLU, tanh, etc.) to the weighted sum of activations of all neurons from the previous layer, and then the obtained activation is transmitted via connections to all neurons in the next layer, all the way to the network output.

The transfer of activations is done in one direction only, from the input to the output of the network, so the MLP structure belongs to the class of feed-forward networks [16].

2.2 Recurrent Neural Networks (RNN)

A recurrent neural network is a network which has neurons that can be connected to neurons within the same layer, to neurons from the previous layer or to itself, unlike the MLP.

Due to such connections, the activation of one neuron depends not only on the network input or activation of neurons from the previous layer, but also on the activations generated by the same neuron at previously brought network inputs.

Thus, the order of input data affects the network output - an input brought in once can affect the output even after specifying a larger number of new inputs after it.

In this way, a network can establish regularities between several consecutive members of an array that are brought to its input.

This is suitable for predicting time series, especially if there is a strong correlation between series members distant for several time moments.

In the simplest structures of RNN networks, data are fed into the inputs in the same order in which they are arranged in sequence, and there is often only one hidden layer within which neurons are connected in the order that accompanies the inputs.

The structure of hidden neurons for a standard RNN is shown in Fig. 1, while Eq. (1) presents the output of the hidden unit of a standard RNN at time t [16].

$$h_t = \tan h(W_x\, x_t + W_h\, h_{(t-1)} + b) \tag{1}$$

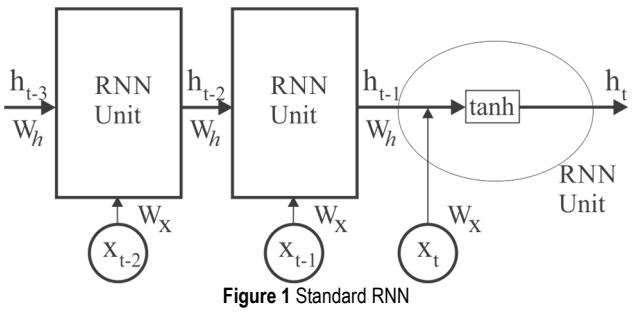

Figure 1 Standard RNN

2.3 Long Short Term Memory (LSTM)

The main disadvantage of standard RNNs is their sensitivity to input sequence length - the effects of inputs from distant moments in the past vanish as they propagate through the network. To reduce prediction errors, RNNs use a BPTT (Backpropagation Through Time) algorithm which modifies the learning gradient for previous input. If the input sequence is too long, the problem of an exploding/vanishing gradient arises, where the learning gradient either diverges or converges rapidly in parts of the network which are at a longer time distance from the output, thus causing the network to stop learning. This makes RNNs successfully applicable only to sequences of short length.

The architecture of LSTMs solves this problem by incorporating a channel called "cell state" along the hidden state channel which is contained in a standard RNN (Fig. 2). The cell state connection spreads across consecutive LSTM cells and is used for passing and updating information relevant to many cells in the chain, regardless of their distance from the current point in time.

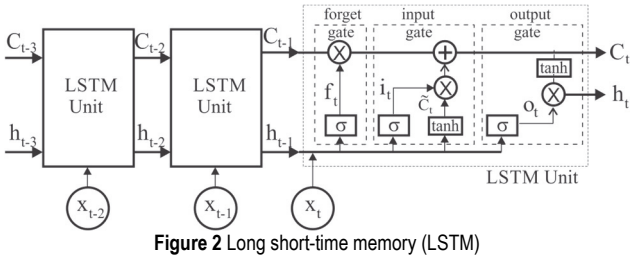

Figure 2 Long short-time memory (LSTM)

The cell state is updated by applying various activation functions and matrix operations on inputs, as well as outputs from the previous time step and the previous cell state. These functions are applied using three activation layers called gates: the forget gate, the input gate, and the output gate. The forget gate regulates the effect of the previous cell state on the next one - it decides whether a piece of information contained in the cell state should be kept or removed (forgotten).

The input gate decides whether the new cell state should be affected by the input, i.e. whether new information based on the input should be added to the cell state or whether the input should be ignored. The output gate makes the prediction, i.e. it determines the information that will be passed to the next LSTM cell depending on the new cell state and the network inputs [17].

2.4 Gated Recurrent Unit (GRU)

Although LSTMs are efficient at solving the vanishing gradient problem, they have many connections and activation function blocks which might degrade the performance of network training in cases of very long input sequences. There are many recurrent network variants based on the structure of LSTMs that can be used to increase training performance and efficiency. One such architecture is the GRU. It merges the LSTM's cell state and the hidden state into one shared connection, and combines the LSTM's forget and input gate into a single update gate, thus decreasing the number of components and connections used (Fig. 3) [18].

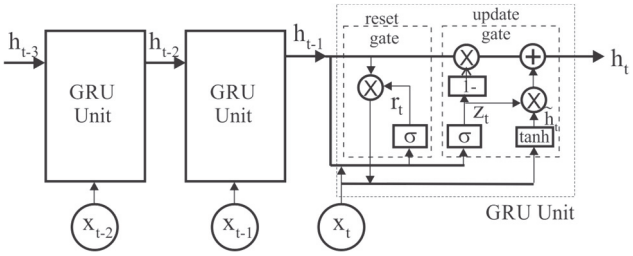

Figure 3 Gated recurrent unit (GRU)

3 CASE STUDY

3.1 Description of the Study Dam

The Bovan dam is built across the river Moravica, a right tributary of the Juzna Morava, 15 km upstream from the town of Aleksinac (Fig. 4).

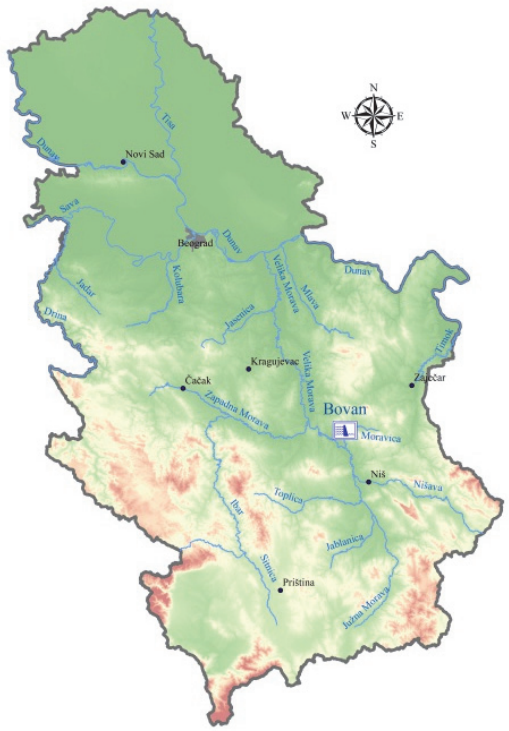

Figure 4 Map with the location of the dam

It is a high embankment rockfill dam with a central clay core and filter zones. The structural height of the dam is 52,4 m and the dam crown is 151 m long. The dam crown elevation is 263,00 m above sea level and the width of the crown is 6,0 m.

The continual monitoring of the high dam behaviour implies dam safety assessment by surveillance, visual observation, and an analysis of the dam response due to implemented static and dynamic load, collected from the installed instruments and devices.

The data processing indicates the dam safety level. Quantifying seepage flows, pore water pressure, and displacements in order to reveal water tightness problems is the main issue for dam safety.

The safety monitoring of the Bovan dam implies collecting hydrometeorological data; hydrogeological data; stress-strain analysis of the dam; absolute and relative displacements of the dam; and appurtenant structures and reservoir silting.

3.2 Database Characteristics

For the geotechnical measurements, eight piezometers in total were used with continual daily data monitoring.

Three piezometers are located on the left bank, while the others are in the dam body. Regarding the cells for measuring pore and total pressure, a large number of cells were destroyed during the construction of the dam.

As a part of the project of revitalization of equipment for technical monitoring of dams, eleven "multi-level" type pore cells were installed, with hourly data reading. In the frame of hydrometeorological measurement (HMM), the following instruments were used: the measuring stream stage for quantifying inflow and outflow from the reservoir, instruments for measuring water level in the reservoir, a thermometer for measuring air temperature, and rain gauges.

Within geotechnical measurement (GM), electrical piezometers were used. Input data for our model are HMM and GM data, namely: the water level in the reservoir (RWL), the piezometer water level (PWL), and air temperature (*T*). The dataset contains a daily situation update over a one-year period. Tab. 1 and Tab. 2 give the dataset range for the reservoir water level, air temperatures, and piezometric water level, respectively. These values are measured daily.

Table 1 Ranges of HMM data

Dataset range	Reservoir water level / masl	Air temperatures / °C
Minimum value	250,84	−6,0
Maximum value	254,05	30,0
Median value	252,24	14,1
Amplitude	3,12	36

Table 2 Ranges of PWL data

Piezometer designation	Dataset range / masl		
	min	max	median
P2	243,72	245,19	244,60
P3	220,20	221,18	220,79
P10	218,43	218,92	218,67
E1	240,19	261,64	256,97
E3	244,52	244,69	244,57
E4	234,95	235,12	235,03
E6	219,32	220,05	219,40
E7	248,61	249,07	248,80

Table 3 Ranges PWP data

PWC designation	PWP range of entire dataset / kPa		
	min	max	median
PC 4-1	−3,1150	2,3759	−0,8561
PC 4-2	7,7666	13,6843	9,5145
PC 4-3	68,4150	78,5858	71,7315
PC 6-1	−4,5278	2,4970	−1,4744
PC 6-2	11,3537	16,7133	13,4061
PC 6-3	55,1417	57,9053	56,4661
PC 6-4	83,9112	86,4787	85,5520
PC 6-5	109,2800	125,6011	113,4981
PC 9-1	−6,8389	−4,1209	−5,6340
PC 9-2	12,5879	17,9056	15,3109
PC 9-3	50,1776	52,8066	51,4253

In Tab. 3, the dataset range for pore pressure is given, while the measurements have an hourly frequency.

We can notice that variations in the water level are slight, as a result of the small amplitude of the RWL of 3,12 m (in the range of the normal water level - NWL).

3.3 Development of Neural Network Models

The aim of this paper is to develop a neural network system that should predict pore pressure based on available measured data (the water level in the reservoir, the piezometer water level, and air temperature).

The clay core is a low permeable dam sealing element and can, due to rising temperature, experience substantial increases in the pore water pressures.

Eq. (2), presents hydraulic conductivity K:

$$K = \frac{k \cdot \rho_w \cdot g}{\mu_w} \tag{2}$$

where:
k - intrinsic permeability / m^2
g - acceleration of gravity / m/s^2
r_w - density of the water / kg/m^3
μ_w - dynamic viscosity of water / kg/ms [19]

The dynamic viscosity of water is inversely proportional to temperature. Besides the measured data, we concluded that a system should also be affected by previous values of pore pressure (values in previous time instants), since their influence is of great importance to the actual values. Based on these presumptions, we created an artificial neural network with all the measured data, including previous pore pressure values as input, and actual pore pressure values as output (11 outputs). The network created in such a way was very robust, and when tested, it did not show satisfactory results.

After analysing these results, we concluded that some inputs had more influence on all the network outputs, which was not the case in reality. This led to bigger values for error and poor prediction. We decided to change this approach, and created a system consisting of 11 neural networks that work in parallel, where each network has fewer inputs and only one output. In other words, we split the previous system into 11 subsystems.

Each subsystem is in charge of one pore pressure only. Thus, the value for one pore pressure is the output of each subsystem. Inputs to each of these systems are measured via piezometer data and temperature (which applies for all the subsystems), and previous data regarding only that pore pressure value. For example, in Fig. 5 we can see the first neural network (NN Unit 11) with pore pressure 11 as its output, the measured data, and the previous data regarding pore pressure 11 as input.

The system has 11 outputs, for 11 pore pressures. Three of them are in cross-section 4a (PC 4-1, PC 4-2, PC 4-3), five are in cross-section 6a (PC 6-1, PC 6-2, PC 6-3, PC 6-4, PC 6-5), and three more are in cross-section 9a (PC 9-1, PC 9-2, PC 9-3) (Fig. 6). These data are available per hour (24 values measured per day). However, in this case, we unfortunately cannot use all these data since we only have one piece of hydrological data available per day. So, we averaged the available data, and used only one value per day for the network training.

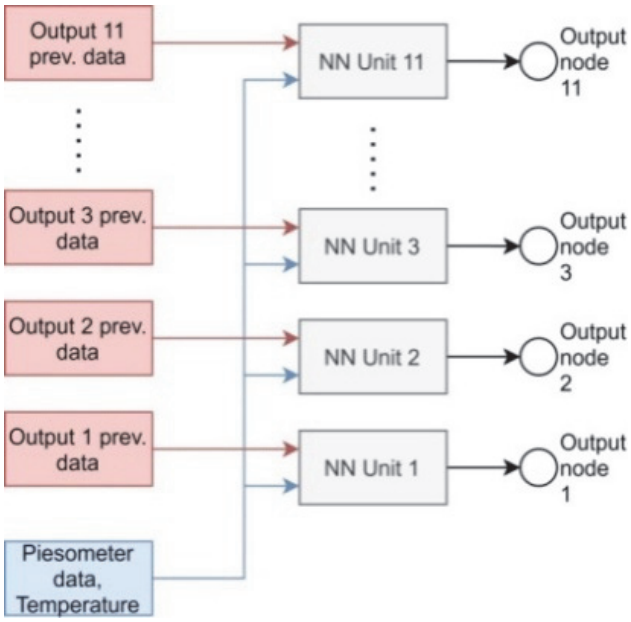

Figure 5 Structure of the overall system

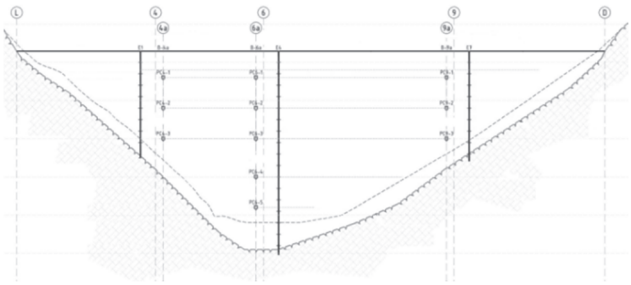

Figure 6 The positions of the pore pressure cells [20]

Table 4 Input data- part of the overall table

Date	RWL / masl	P2 / masl	P3 / masl	P10 / masl	E1 / masl	E3 / masl	E4 / masl	E6 / masl	E7 / masl	T / °C
Dec 22	250,89	243,80	220,21	218,49	248,86	244,54	235,07	219,11	248,64	15
Dec 23	250,91	243,80	220,22	218,48	249,12	244,54	235,06	219,11	248,65	16
Dec 24	250,93	243,80	220,22	218,48	249,38	244,55	235,05	219,11	248,65	17
Dec 25	250,96	243,80	220,21	218,48	249,64	244,55	235,04	219,11	248,65	6
Dec 26	250,99	243,80	220,21	218,47	249,9	244,55	235,03	219,12	248,66	7
Dec 27	251,03	243,81	220,21	218,47	250,16	244,56	235,02	219,12	248,66	6
Dec 28	251,03	243,81	235,20	218,47	250,42	244,56	235,01	219,12	248,67	4
Dec 29	251,04	243,81	220,20	218,46	250,68	244,57	235,01	219,12	248,67	5
Dec 30	251,05	243,81	220,20	218,46	250,94	244,57	235,00	219,12	248,67	-1
Dec 31	251,05	243,82	220,20	218,46	251,20	244,57	235,00	219,12	245,67	-3

In Tab. 5, such data for a 12-hour period (Dec 31st) is given, and we can see the average value in the last line.

The average value of the daily measurements (24 hours) from November 5th to October 1st was used in the neural network training process. Usually the training set makes up 70% of all the data, and the test set takes up the rest [21].

In total, we obtained 32 different structures (8 for every network type), and the obtained results are analysed in the remaining text.

Each of these structures has 10 inputs, as given in Tab. 4. Furthermore, each network has additional inputs, depending on its structure. For example, if we take into account one previous day, that network will have 1 additional input, as the pore pressure value for the previous day.

If we take into account two previous days, that network will have 2 additional inputs, as the pore pressure values for two previous days, and so on.

Each of these structures has 11 outputs, as given in Tab. 5. We used structures with 2 hidden layers, each with 128 hidden neurons.This number of hidden neurons was selected after testing models with different numbers of neurons in the hidden layers.

The training process consisted of the iterative optimization of network parameters in order to obtain the minimal root mean square error between the expected and predicted values.

The network models used in this paper are described in Python 3.7.9, using the Keras deep learning API from the TensorFlow platform for machine learning [22].

Table 5 Output data- part of the overall table

Time / h	PC 4-1 / kPa	PC 4-2 / kPa	PC 4-3 / kPa	PC 6-1 / kPa	PC 6-2 / kPa	PC 6-3 / kPa	PC 6-4 / kPa	PC 6-5 / kPa	PC 9-1 / kPa	PC 9-2 / kPa	PC 9-3 / kPa
0.00	1,4492	10,6482	75,9358	1,5571	16,2086	56,1733	86,3977	118,3395	−5,1116	17,0571	51,4197
1.00	1,3957	10,6413	75,9186	1,5020	16,2040	56,1703	86,3927	118,3294	−5,1092	17,0524	51,4172
2.00	1,3892	10,6380	75,9260	1,4948	16,2072	56,1728	86,3959	118,3300	−5,1065	17,0498	51,4501
3.00	1,3259	10,6322	75,9200	1,4291	16,2022	56,1697	86,3897	118,3201	−5,1049	17,0467	51,5261
4.00	1,2750	10,6273	75,9193	1,3784	16,2003	56,1692	86,3892	118,3161	−5,1032	17,0433	51,5063
5.00	1,2458	10,6248	75,9177	1,3523	16,2022	56,1697	86,3877	118,3122	−5,1015	17,0408	51,4917
6.00	1,2287	10,6225	75,9126	1,3317	16,2051	56,1712	86,3885	118,3115	−5,1004	17,0394	51,4803
7.00	1,1994	10,6188	75,9109	1,3018	16,2064	56,1728	86,3885	118,3080	−5,0994	17,0377	51,4682
8.00	1,1648	10,6166	75,9102	1,2690	16,2045	56,1697	86,3857	118,3020	−5,0987	17,0359	51,4599
9.00	1,1637	10,6173	75,9157	1,2678	16,2072	56,1754	86,3865	118,3020	−5,0978	17,0355	51,4555
10.00	1,1317	10,6156	75,9052	1,2328	16,2024	56,1700	86,3820	118,2950	−5,0999	17,0333	51,4494
11.00	1,0355	10,6082	75,8944	1,1428	16,1962	56,1610	86,3726	118,2779	−5,1015	17,0301	51,4418
12.00	0,9161	10,5994	75,8847	1,0368	16,1894	56,1553	86,3636	118,2640	−5,1049	17,0247	51,4336
Average	1,0153	10,6069	75,8928	1,1182	16,1974	56,1671	86,3780	118,2816	−5,1155	17,0287	51,4443

4 RESULTS AND DISCUSSION

The RMSE values for all the models are given in Tabs. 6, 7, 8, and 9, for every network output.

At first glance, we can note from these tables that the errors are significantly greater for PC 4-1 and PC 6-1, and not so great, but greater than the others, for PC 9-1.

We tried to analyse this phenomenon, and concluded that three PWPCs (PC 4-1, PC 6-1, and PC 9-1) were all installed above the NWL; thus, the instruments read capillary water.

The pressure registered on the PWPC has a negative value.

Table 6 RMSE for all outputs for various numbers of previous days, the MLP model

Days	PC 4-1	PC 4-2	PC 4-3	PC 6-1	PC 6-2	PC 6-3	PC 6-4	PC 6-5	PC 9-1	PC 9-2	PC 9-3
1	28,692	2,132	0,353	18,602	0,903	0,035	0,319	0,458	2,066	0,506	0,034
3	24,557	0,450	0,097	15,650	0,500	0,042	0,097	0,206	3,451	0,695	0,064
5	24,200	0,912	0,094	16,298	0,678	0,049	0,115	0,093	2,416	0,889	0,096
10	24,557	3,020	0,087	16,871	1,420	0,096	0,233	0,113	2,880	1,044	0,112
15	25,609	3,675	0,053	17,814	2,109	0,078	0,159	0,089	2,853	1,893	0,138
20	25,326	2,700	0,082	17,898	1,477	0,060	0,145	0,119	2,658	3,074	0,192
25	24,553	4,694	0,257	17,920	1,442	0,062	0,186	0,167	2,039	3,534	0,109
30	25,041	0,926	0,278	15,396	3,664	0,071	0,116	0,074	3,191	2,654	0,137

Table 7 RMSE for all outputs for various numbers of previous days, the RNN model

Days	PC 4-1	PC 4-2	PC 4-3	PC 6-1	PC 6-2	PC 6-3	PC 6-4	PC 6-5	PC 9-1	PC 9-2	PC 9-3
1	27,217	2,184	0,857	14,440	0,516	0,034	0,277	0,186	1,320	0,638	0,060
3	24,780	0,722	0,215	20,628	0,202	0,076	0,168	0,051	3,012	0,999	0,070
5	27,152	0,789	0,113	14,689	0,348	0,111	0,252	0,096	2,443	1,260	0,157
10	25,946	2,527	0,200	15,599	1,312	0,112	0,121	0,155	2,780	1,674	0,219
15	25,256	2,400	0,143	13,920	2,480	0,213	0,060	0,095	2,395	3,353	0,218
20	24,458	0,741	0,130	16,412	1,420	0,132	0,070	0,070	2,852	1,896	0,390
25	23,991	2,839	0,325	22,079	0,274	0,145	0,045	0,102	3,347	4,351	0,416
30	27,292	0,855	0,608	25,102	4,130	0,267	0,119	0,169	3,615	1,956	0,117

Table 8 RMSE for all outputs for various numbers of previous days, the LSTM model

Days	PC 4-1	PC 4-2	PC 4-3	PC 6-1	PC 6-2	PC 6-3	PC 6-4	PC 6-5	PC 9-1	PC 9-2	PC 9-3
1	28,411	3,509	0,407	18,172	1,157	0,058	0,158	0,491	1,107	1,465	0,451
3	24,842	1,318	0,539	17,251	0,536	0,064	0,127	0,197	2,182	0,803	0,135
5	23,017	0,674	0,499	17,685	0,484	0,054	0,187	0,190	2,218	1,125	0,119
10	24,732	2,508	0,351	20,940	0,889	0,073	0,218	0,119	2,096	1,591	0,064
15	24,627	1,817	0,351	19,781	1,090	0,055	0,223	0,066	2,418	1,918	0,058
20	24,916	2,158	0,307	15,222	1,482	0,055	0,196	0,089	2,521	2,727	0,091
25	25,529	1,987	0,392	28,794	1,879	0,092	0,170	0,076	2,631	2,753	0,068
30	26,772	0,695	0,415	31,345	1,589	0,122	0,102	0,120	3,055	3,708	0,084

Table 9 RMSE for all outputs for various numbers of previous days, the GRU model

Days	PC 4-1	PC 4-2	PC 4-3	PC 6-1	PC 6-2	PC 6-3	PC 6-4	PC 6-5	PC 9-1	PC 9-2	PC 9-3
1	27,545	4,338	1,008	18,366	0,769	0,085	0,157	0,453	1,157	0,870	0,096
3	24,489	1,711	0,502	17,961	0,455	0,049	0,129	0,263	2,478	0,845	0,064
5	25,437	0,468	0,450	18,418	0,471	0,112	0,142	0,144	2,549	1,107	0,064
10	24,988	2,054	0,232	18,245	1,389	0,084	0,192	0,109	2,080	2,081	0,068
15	24,600	0,826	0,197	20,514	1,431	0,080	0,182	0,092	2,645	2,302	0,186
20	24,261	2,590	0,312	18,171	1,557	0,076	0,100	0,088	2,394	2,359	0,122
25	23,917	1,549	0,344	22,418	1,839	0,056	0,073	0,128	2,598	3,585	0,165
30	26,852	1,158	0,309	26,028	1,524	0,061	0,158	0,066	2,659	2,256	0,347

The crest of the dam is not subjected to severe hydraulic pressure even in extreme hydrologic conditions. So, we did not find these data necessary. In Tab. 10, we extracted mean error values for each network type and structure.

For each type, the minimum value is bolded. The overall minimum mean error value was obtained for the MLP network type (4,165).

A very interesting finding is that minimum errors are obtained for 3 and 5 previous days, depending on the network type.

This means that we get better results with simpler network structures, which facilitates and speeds up the forecast process.

The error is calculated for PC 4-2, PC 4-3, PC 6-2, PC 6-3, PC 6-4, PC 6-5, PC 9-2, and PC 9-3 (not for all points) (Tab. 11).

From these tables we can see that the error is now significantly lower, with maximum values of around 1%.

The minimum error was obtained for pore pressure values from 3 and 5 previous days, while the overall minimum error value was obtained for the MLP network type.

So, the general conclusions remain the same.

From both Tabs. 10 and 11 we can see that the smallest RMSE is obtained for the MLP network, when data for pore pressure from 3 previous days are included in the model.

We can conclude that this is the best model, which also has the simplest structure.

In Figs. 7 to 14 we present the expected vs. predicted values for this network.We have successfully predicted values for a period of more than 90 days, and from the figures we can note that the obtained errors are negligible, as stated in the tables.

Table 10 Mean error values for each network type and structure / %

No. of previous days	MLP	RNN	LSTM	GRU
1	4,918	4,339	5,035	4,986
3	**4,165**	4,629	4,363	**4,450**
5	4,167	**4,310**	**4,205**	4,487
10	4,585	4,604	4,871	4,684
15	4,952	4,594	4,764	4,823
20	4,885	4,416	4,524	4,730
25	4,997	5,265	5,852	5,152
30	4,686	5,839	6,182	5,584

Table 11 Mean error values for each network type and structure, calculated without PC 4-1, PC 6-1, and PC 9-1 / %

No. of previous days	MLP	RNN	LSTM	GRU
1	0,593	0,594	0,962	0,972
3	0,269	0,313	0,465	0,502
5	0,366	0,391	0,417	0,370
10	0,766	0,790	0,726	0,776
15	1,024	1,120	0,697	0,662
20	0,981	0,606	0,888	0,901
25	1,306	1,062	0,927	0,967
30	0,990	1,028	0,854	0,735

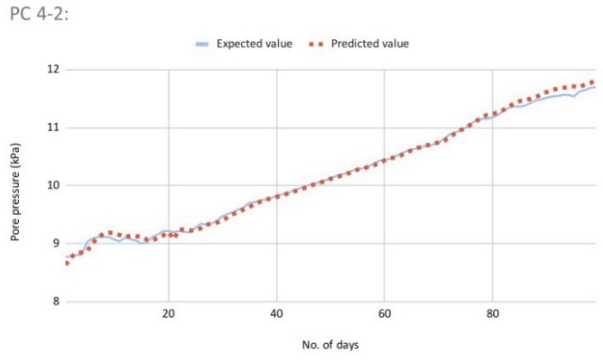

Figure 7 Expected vs. predicted value for PC 4-2

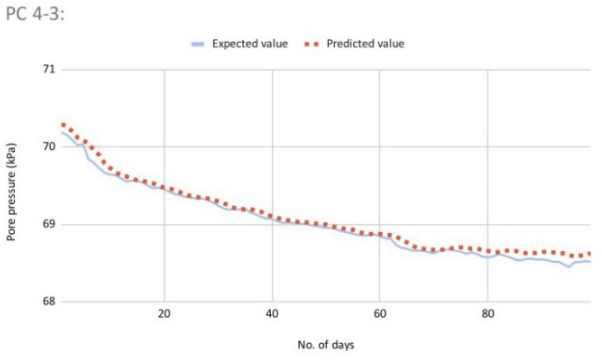

Figure 8 Expected vs. predicted value for PC 4-3

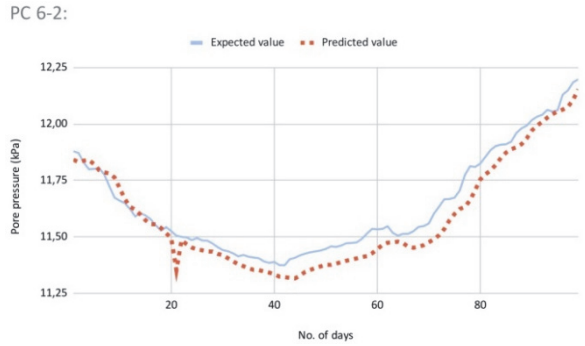

Figure 9 Expected vs. predicted value for PC 6-2

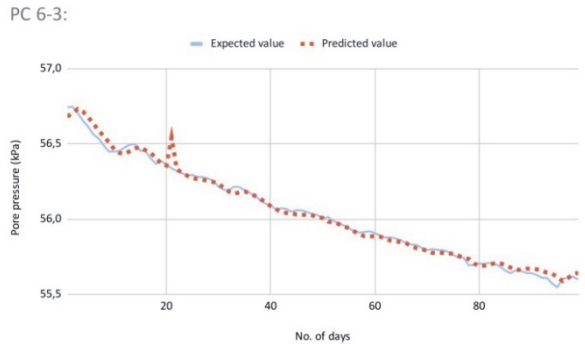

Figure 10 Expected vs. predicted value for PC 6-3

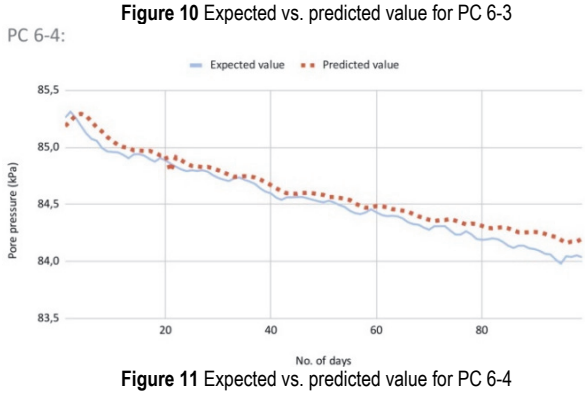

Figure 11 Expected vs. predicted value for PC 6-4

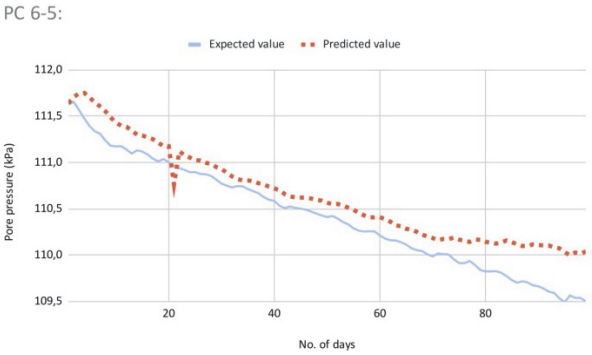

Figure 12 Expected vs. predicted value for PC 6-5

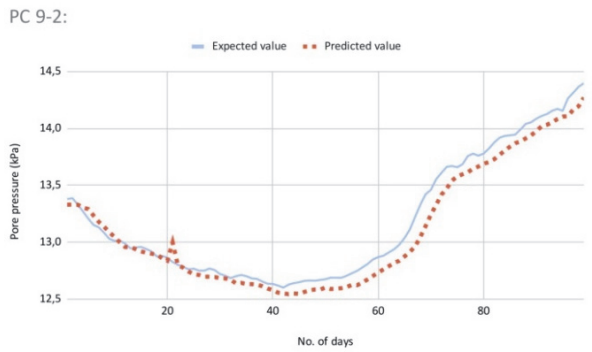

Figure 13 Expected vs. predicted value for PC 9-2

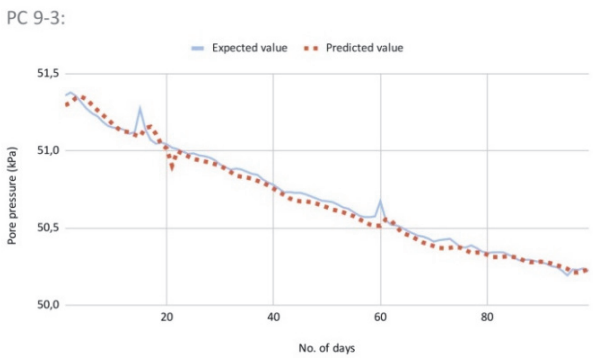

Figure 14 Expected vs. predicted value for PC 9-3

We can also note that the graph which gives expected values is tracked both in its shape and its values.

5 CONCLUSION

In this paper we tried to determine a correlation between pore pressure and hydrological data using different structures of artificial neural networks. Based on this correlation, an ANN can predict pore water pressure when hydrological, meteorological, and geotechnical datasets are available, or can assume what their values will be.

The obtained results show that a prediction can be made with negligible errors. In the process of obtaining these results, we noted that data from some of the PWPCs lead to a significant error, so in our future work we will exclude these data, as they have proved not to be significant for our model. These data are obtained from the PWPCs that are installed above the normal water level.

This method can be used for PWPC data prediction in extreme weather events, i.e. in the spring when the water level in the reservoir is in an extreme interval. This period is usually early springtime (March and April), the rainiest season in the Northern Hemisphere, as measured by the number of days with precipitation. In Serbia, annual springtime flood events are often known as rain-on-snow events. With a piezometric water level dataset in the dam body, any behaviour of the PWPC dataset can be analysed separately, defining the "weak points" and possible cracks in the dam clay core.

Predicting PWP data is extremely important for dam sensitivity analysis in order to define possible rehabilitation measures to increase the stability of the dam and related public safety.

6 REFERENCES

[1] Markovic, M., Brankovic, J., Stosovic, M., Zivkovic, S., & Brankovic, B. (2021). A New Method for Pore Pressure Prediction on Malfunctioning Cells Using Artificial Neural Networks. *Water Resources Management*, *35*(3), 979-992. https://doi.org/10.1007/s11269-021-02763-0

[2] Akpınar, B. (2015). Online system for monitoring the safety of engineering structures. *Tehnicki Vjesnik - Technical Gazette*, *22*(1), 217-225. https://doi.org/10.17559/TV-20150101150810

[3] Pagano, L. et al. (2010). Pore water pressure measurements in the interpretation of the hydraulic behaviour of two earth dams. *Soils and Foundations,* 50(2), 295-307. https://doi.org/10.3208/sandf.50.295

[4] Xu, J., Wei, W., Bao, H., Zhang, K., Lan, H., Yan, C., & Sun, W. (2019). Failure models of a loess stacked dam: a case

study in the Ansai Area (China). *Bulletin of Engineering Geology and the Environment*, *79*(2), 1009-1021. https://doi.org/10.1007/s10064-019-01605-z

[5] Ahmed, A., Elkatatny, S., Ali, A., Mahmoud, M., & Abdulraheem, A. (2018). New Model for Pore Pressure Prediction While Drilling Using Artificial Neural Networks. *Arabian Journal for Science and Engineering*, *44*(6), 6079-6088. https://doi.org/10.1007/s13369-018-3574-7

[6] Jin, J., Cui, H., Liang, L., Li, S., & Zhang, P. (2018). Variation of Pore Water Pressure in Tailing Sand under Dynamic Loading. *Shock and Vibration*, *2018*, 1-13. https://doi.org/10.1155/2018/1921057

[7] Chiaradonna, A., Flora, A., d'Onofrio, A., & Bilotta, E. (2020). A pore water pressure model calibration based on in-situ test results. *Soils and Foundations*, *60*(2), 327-341. https://doi.org/10.1016/j.sandf.2019.12.010

[8] Markovic Brankovic, J., Markovic, M., Andrejevic Stosovic, M., Zivkovic, S., & Brankovic, B. (2021). ANN Model for Prediction of Rockfill Dam Slope Stability. *Tehnički vjesnik, 28*(5), 1488-1494. https://doi.org/10.17559/TV-20200707150903

[9] Akhtarpour, A. & Salari, M. (2018). The Deformation Mechanism of a High Rockfill Dam during the Construction and First Impoundin. *Scientia Iranica*. https://doi.org/10.24200/sci.2018.20778

[10] Aniskin, N., Rasskazov, L., & Yadgorov, E. (2016). Seepage and Pore Pressure in the Core of a Earth-and-Rockfill Dam. *Power Technology and Engineering*, *50*(4), 378-384. https://doi.org/10.1007/s10749-016-0717-4

[11] Aniskin, N., Rasskazov, L., & Yadgorov, E. (2017). Filtration, Pore Pressure, and Settling From Consolidation of an Ultra-High Dam. *Power Technology and Engineering*, *50*(6), 600-605. https://doi.org/10.1007/s10749-017-0757-4

[12] Baum, R., Savage, W., & Godt, J. (2008). TRIGRS - A Fortran Program for Transient Rainfall Infiltration and Grid-Based Regional Slope-Stability Analysis, Version 2.0. *Open-File Report*. https://doi.org/10.3133/ofr20081159

[13] Ng, C., Liu, H., & Feng, S. (2015). Analytical solutions for calculating pore-water pressure in an infinite unsaturated slope with different root architectures. *Canadian Geotechnical Journal*, *52*(12), 1981-1992. https://doi.org/10.1139/cgj-2015-0001

[14] Gao, X., Liu, H., Zhang, W., Wang, W., & Wang, Z. (2018). Influences of reservoir water level drawdown on slope stability and reliability analysis. *Georisk: Assessment and Management of Risk for Engineered Systems and Geohazards*, *13*(2), 145-153. https://doi.org/10.1080/17499518.2018.1516293

[15] Shibata, T., Shuku, T., Murakami, A., Nishimura, S. I., Fujisawa, K., Hasegawa, N., & Nonami, S. (2019). Prediction of long-term settlement and evaluation of pore water pressure using particle filter. *Soils and Foundations*, *59*(1), 67-83. https://doi.org/10.1016/j.sandf.2018.09.006

[16] Haykin, S. (2008). *Neural Networks and Learning Machines*. Pearson, Prentice Hall

[17] Hochreiter, S. & Schmidhuber, J. (1997). Long Short-Term Memory. *Neural Computation*, *9*(8), 1735-1780. https://doi.org/10.1162/neco.1997.9.8.1735

[18] Wang, J., Guo, C., & Wu, L. (2021). Gated Recurrent Unit with RSSIs from Heterogeneous Network for Mobile Positioning. *Mobile Information Systems*, *2021*, 1-7. https://doi.org/10.1155/2021/6679398

[19] Dassargues, A. (2018). *Hydrogeology: Groundwater science and engineering (1st ed.)*. CRC Press. https://doi.org/10.1201/9780429470660

[20] Jaroslav Cerni Water Institute. (2014). *Dam "Bovan", Main Design of modernization of technical observation (p. Anex 5).* Belgrade

[21] Evaluating a machine learning model. (2021).

[22] Tensor flow. Tensor Flow. (n.d.).

Contact information:

Dr Milica MARKOVIC, Assistant Professor
(Corresponding author)
Faculty of Civil Engineering and Architecture, University of Nis,
Aleksandra Medvedeva 14, 18000 Nis, Republic of Serbia
E-mail: milica.markovic@gaf.ni.ac.rs

Novak RADIVOJEVIC, MSc
Faculty of Electronic Engineering, University of Nis,
Aleksandra Medvedeva 14, 18000 Nis, Republic of Serbia
E-mail: novak.radivojevic@elfak.ni.ac.rs

Dr Miona ANDREJEVIC STOSOVIC, Associate Professor
Faculty of Electronic Engineering, University of Nis,
Aleksandra Medvedeva 14, 18000 Nis, Republic of Serbia
E-mail: miona.andrejevic@elfak.ni.ac.rs

Dr Jelena MARKOVIC BRANKOVIC, Associate Professor
Faculty of Civil Engineering and Architecture, University of Nis,
Aleksandra Medvedeva 14, 18000 Nis, Republic of Serbia
E-mail: jelena.markovic.brankovic@gaf.ni.ac.rs

Dr Srdjan ZIVKOVIC, Associate Professor
Faculty of Civil Engineering and Architecture, University of Nis,
Aleksandra Medvedeva 14, 18000 Nis, Republic of Serbia
E-mail: srdjan.zivkovic@gaf.ni.ac.rs